ILASS Americas, 19th Annual Conference on Liquid Atomization and Spray Systems, Toronto, Canada, May 2006

Effect of Droplet Distortion on the Drag Coefficient in Accelerated Flows

Shaoping Quan, S. Gopalakrishnan and David P. Schmidt*
Department of Mechanical and Industrial Engineering
University of Massachusetts - Amherst
Amherst, MA 01003 USA

Abstract

The distortion of a liquid droplet from its spherical shape has a profound influence on its drag coefficient. The areas of greatest uncertainty are the drag at high Reynolds and Weber numbers as well as acceleration and history effects. Though several reduced models have been developed for use in spray modeling, a detailed, direct numerical simulation offers the opportunity to learn more about the underlying physics. A numerical investigation has been performed to study the variation of the droplet drag with change in deformation factor of the liquid drop, and to better understand the dependence on Ohnesorge number and acceleration. The transient nature of these simulations will advance the understanding of flow effects on the droplet drag.

Introduction

The accuracy of any spray model depends greatly on the correctness of the drag coefficient computed for the liquid droplets. Experiments have shown that droplets having a Weber number significantly larger than unity tend to deform, which results in a change in their drag characteristics. The distortion of the droplet causes the increase in the frontal projected area, causing a deviation from the ideal spherical drag characteristics.

Until recently droplet distortion and its effect on drag characteristics have been studied experimentally using wind tunnels [1] and shock tube experiments [2]. A summary of these experiments and the correlations obtained by them can be found in [3]. These experiments are limited by the range of droplet sizes, fluid densities and viscosities being investigated. A numerical study is posed with no such challenges and offers a greater degree of control in the simulation parameters. An arbitrary Lagrangian Eulerian approach with an adaptive remeshing scheme was used in [4] to simulate two-dimensional quasi-steady flow around liquid droplets. This method was successful in handling large deformation of the interface. Three-dimensional computations have typically found it difficult to reliably handle large interfacial deformations without running into significant numerical errors.

In this paper, we use a moving mesh based approach with an adaptive remeshing scheme [5]. A 3D unstructured finite volume scheme is used to perform the simulation. The interface is tracked in a Lagrangian manner in a deforming tetrahedral mesh. This approach gives us the advantage of exactly tracking the interface within the limits of discretization error. An adaptive mesh refinement scheme is implemented in order to maintain the quality of mesh. The adaptation involves mesh flipping, edge collapse and edge bisection algorithms. An optimization based smoothing algorithm is used in conjunction with the mesh adaptation schemes.

Here, we present a preliminary report on the effect of droplet distortion on its drag coefficient. Our approach helps us to closely correlate the deformation of a liquid droplet to the drag coefficient. The transient nature of the simulation will help us better understand the effect of flow history on the drag coefficient. At this juncture, we are just beginning to investigate the parameter space and the early results provide new insight into the drag characteristics which have not yet been unearthed by experimental data.

Governing equations and Discretization

The governing equations for the moving and deforming control volume are described by the following set of equations.

$$\frac{dV}{dt} = \iint_{CS} \mathbf{v} \cdot \mathbf{n} ds \tag{1}$$

Eqn. (1) represents the conservation of volume for a distorting control volume.

$$\frac{d}{dt} \iiint_{CV} \rho dv + \iint_{CS} \rho(\mathbf{u}\text{-}\mathbf{v}) \cdot \mathbf{n} ds = 0 \tag{2}$$

Eqn. (2) denotes the conservation of mass and Eqn. (3) gives the conservation of momentum.

$$\begin{aligned} &\frac{d}{dt} \iiint_{CV} \rho \mathbf{u} dv + \iint_{CS} \rho \mathbf{u}(\mathbf{u}\text{-}\mathbf{v}) \cdot \mathbf{n} ds = \\ &\iiint_{CV} \rho \mathbf{f} dv - \iiint_{CV} \nabla p dv + \iint_{CS} \mu(\nabla \mathbf{u} + \nabla \mathbf{u}^T) \cdot \mathbf{n} ds \end{aligned} \tag{3}$$

In the above equations *CV* stands for the control volume, *CS* the control surface, **u** is the fluid velocity, **v** the velocity of the control surface, **n** is the unit vector of the face normal and **f** denotes the body force per unit mass.

The two phases are assumed to be incompressible and immiscible. The continuity and jump conditions across the interface are given by the following equations.

$$u_{1n} = u_{2n} = v_n \tag{4}$$

$$[\![u_t]\!] = 0 \tag{5}$$

$$[\![p]\!] = -\sigma(\frac{1}{R_1} + \frac{1}{R_2}) + [\![2\mu(\nabla \mathbf{u} \cdot \mathbf{n}) \cdot \mathbf{n}]\!] \tag{6}$$

$$\left[\!\!\left[\mu(\frac{\partial u_i}{\partial x_j} + \frac{\partial u_j}{\partial x_i}) \tau_i n_j \right]\!\!\right] = 0 \tag{7}$$

where σ is assumed to be the constant surface tension, R_1 and R_2 denote the radii of curvature and τ is the tangential vector. Eqn. (4) states that the normal velocities of both the fluids at the interface are equal and same as the normal velocity of the moving mesh. The continuity in the tangential velocity across the interface is given by Eqn. (5). The pressure jump balanced by the surface tension is denoted by Eqn. (6). The continuity of the viscous shear stresses across the interface is described by Eqn. (7).

The governing equations (1),(2) and (3) are discretized as given in [6].

$$\frac{V_c^{n+1} - V_c^n}{\Delta t} = \sum_{cell\ faces} U_f^{mesh} \tag{8}$$

$$\frac{\rho_c^{n+1} V_c^{n+1} - \rho_c^n V_c^n}{\Delta t} + \sum_{cell\ faces} \rho_f (U_f - U_f^{mesh}) = 0 \tag{9}$$

$$\frac{\rho_c^{n+1}\mathbf{u}_c^{n+1}V_c^{n+1}-\rho_c^{n}\mathbf{u}_c^{n}V_c^{n}}{\Delta t}+\sum_{\text{cell faces}}\rho_f\mathbf{u}_f(U_f-U_f^{mesh})$$
$$=-V_c\nabla(p-\rho\mathbf{g}\cdot\mathbf{r}_c^{CG})+\sum_{\text{cell faces}}\mu(\nabla\mathbf{u}+\nabla\mathbf{u}^T)\cdot\mathbf{n}_f A_f \quad (10)$$
$$-V_c(\mathbf{g}\cdot\mathbf{r}_c^{CG})\nabla\rho$$

where V_c is the cell volume, U_f denotes the face flux, U_f^{mesh} the equivalent mesh flux of the face, A_f is the face area, $\mathbf{r}_c^{CG}$ denotes the position of cell center and g is gravitational force per unit mass. Subscript n is the time step.

Simulation Setup

In the numerical investigations both the fluids are assumed to be incompressible, to have constant densities ρ_g and ρ_l, and constant viscosities, μ_g and μ_l for the gas and liquid phases respectively. The surface tension at the interface of the two fluids σ is assumed to be a constant.

The deformation factor D is defined as the ratio of the shortest axis to that of the longest axis of the deformed droplet. The Reynolds number is based on the relative velocity and the gas phase properties and is given by,

$$\mathrm{Re}_g=\frac{\rho_g\left(U_g-U_l\right)2r_0}{\mu_g} \quad (11)$$

The general drag force on the droplet is given by the Basset-Boussinesq-Oseen (BBO) equation, which is too complex for use in applied CFD simulations with large numbers of parcels. The drag force includes the aerodynamic steady-state drag, added mass forces, pressure gradient forces, and a history integral. However, in typical CFD analyses where the droplet is considered to be a point mass, numerous terms of this equation may be neglected [3]. Typically, only the steady state drag is used in order to define a coefficient of drag.

$$C_D=\frac{\frac{8}{3}\eta\, r_0\frac{dU_l}{dt}}{(U_g-U_l)^2} \quad (12)$$

where $\eta=\rho_l/\rho_g$ is the density ratio between liquid and gas phases. This definition presumes that drag is equal to the steady state value and that the droplet may be represented as a sphere. The following detailed simulations will report the acceleration non-dimensionalized as in Eqn. (12). These values of C_D are what a typical CFD code would have to use in order to predict droplet acceleration correctly. These results are not intended to validate the correctness of Eqn. (12) for general use.

Case 1. This simulation is setup to mimic a shock tube experiment. A stationary liquid droplet is suddenly put under the influence of a gaseous flow and is impulsively accelerated. The density and viscosity ratios maintained between the liquid phase and the gas phase are 50.

The computational domain is box with a spherical droplet of radius r_o located at the center of the box. The length of the box is $48r_o$, the width and height are $16r_o$. Boundary effects are neglected since the box is large compared to spherical droplet. An inlet boundary condition is enforced on the right side of the domain and an exit boundary condition is set on the left side of the domain.

Initially the velocity in the liquid phase is set to zero and a constant velocity is given to the gas phase in order to achieve a uniform velocity field. Since the velocity is not continuous across the interface large velocity errors will occur as shown in Figure 1. To alleviate this problem the simulation is run with the droplet being treated as a fixed solid until the velocity jump is smoothed out by the viscosity as shown in Figure 2.

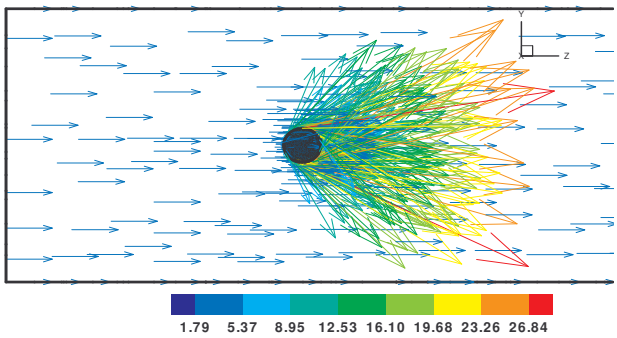

Figure 1: Initial velocity field with stream function discontinuities across the interface

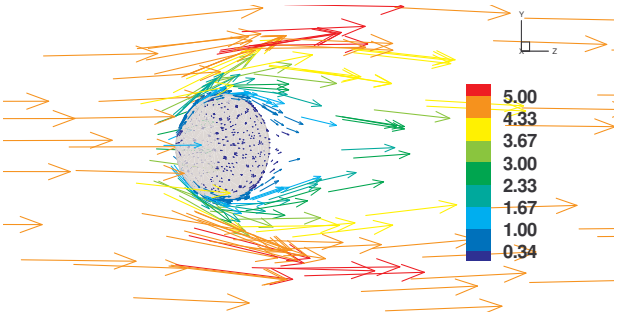

Figure 2: Velocity field smoothed out by viscosity.

Case 2. Here a wind tunnel experiment [1] is simulated in which a droplet is injected in a converging wind tunnel and then subjected to an accelerating flow. It is

computationally very expensive and inefficient to perform a complete direct numerical simulation of a liquid droplet in a wind tunnel. In this setup as well the computational domain is a box with a liquid droplet centered in it.

The computational domain is translated along with the liquid droplet in such a manner that the droplet is always centered. An inlet boundary condition is enforced on the left side on the domain. The initial condition imposed on the domain is similar to that of case 1. The same procedure to smooth velocities at the interface is followed. The velocity inlet boundary condition is continuously varied with time according the rules of flow in converging nozzles. An exit condition is prescribed to the right of the domain and the remaining walls are modeled as slip walls. In this case the density and viscosity ratios maintained are 100 between the liquid phase and the gas phase.

Results

As the droplet is impulsively accelerated by the gaseous flow the initial Reynolds number and Weber number are 40. During the acceleration of the droplet, it continuously deforms, the shape of the liquid droplet at various times is given in Figure 7. The deformation rate of the droplet is initially high and reduces as the relative velocity between the gas and the droplet decreases. The variation of the deformation factor with time is given in Figure 3.

The Reynolds number based on the gas velocity goes down as the liquid phase catches up with gas phase. This results in the reduction on the drag coefficient over time. Figure 4 and Figure 5 confirm this trend. These simulation results prove that the droplet deformation significantly affects the drag characteristics.

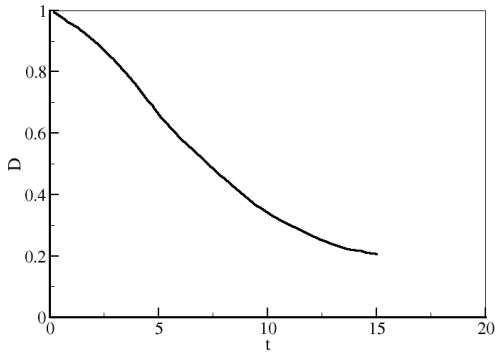

Figure 3: Variation of deformation factor with time.

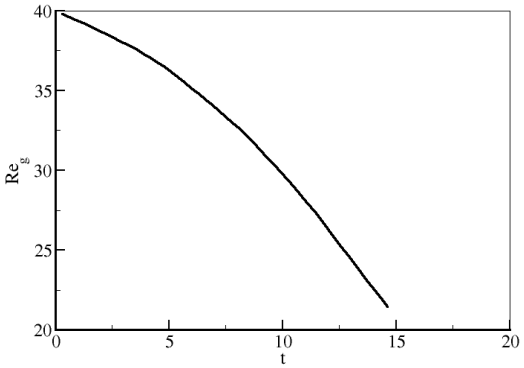

Figure 4: Reynolds number vs. time

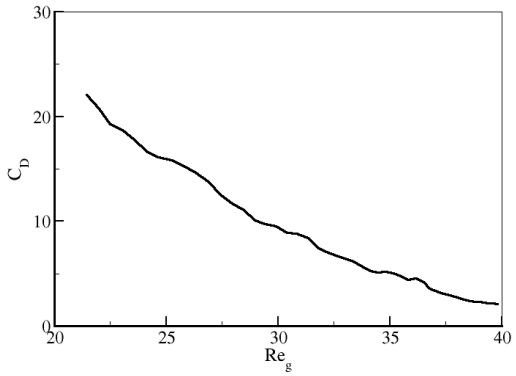

Figure 5: Coefficient of Drag based on initial drop radius vs. Reynolds number

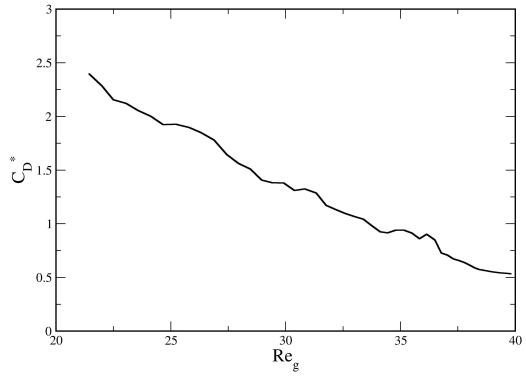

Figure 6: Coefficient of Drag based on frontal projection area vs. Reynolds number

The C_D is computed on the basis of the initial drop radius where as C_D^* is the drag coefficient which is based on the frontal projection area. The volume of the liquid droplet will remain constant; therefore the frontal projection area can be calculated using the deformation factor data by assuming the droplet to be a prolate spheroid. It is evident that the drag predicted is much higher than the standard drag measured by experiments but correlates well with experimental data from [2]. One of the reasons for the higher drag coefficient is the larger

deformation predicted by the simulation compared to the experiment. The numerical investigations validate the belief that the unsteady drag in accelerating flows is larger than steady drag.

For the second case where the droplet is injected in a wind tunnel, the initial trends show a similar pattern where the predicted drag coefficients are higher than the ones suggested by currently accepted drag models. This needs to be firmly established by running the simulation over a larger time frame.

Conclusions

Numerical investigations were performed to study the drag characteristics of deforming droplets in accelerating flows. The increased frontal area due to the deformation causes an increase in the drag coefficient which is significantly higher than the values proposed by conventional drag models. These preliminary simulation results confirm this upward trend in the prediction of droplet drag. Further investigations are needed to study a larger range of flow conditions and the related history effects.

Acknowledgements

This work was performed with the support of the Office of Naval Research under contract N00014-02-1-0507. We also thank J. Blair Perot at University of Massachusetts – Amherst for sharing hardware and software resources.

References

1. Luxford, G.,Hammond, D.W., and Ivey, P., *Forty Second AIAA Aerospace and Sciences Meeting and Exhibit*, Reno, Nevada, USA, January 2004.
2. Temkin, S., and Kim, S.S., *Journal of Fluid Mechanics* 96:133-157 (1980).
3. Clift, R., Grace, J.R., and Weber, M.E., *Bubbles, Drops and Particles*, Academic Press, 1978.
4. Helenbrook, B.T., and Edwards, C.F., *International Journal of Multiphase Flow* 28:1631-1657 (2002)
5. Dai, M., Quan, S., and Schmidt, D.P., *17th Annual Conference of ILASS-Americas: Institute of Liquid Atomization and Spray Systems*, Arlington, Virginia, USA, May, 2004.
6. Perot, J.B., and Nallapati, R., *Journal of Computational Physics* 184:192-214 (2003).

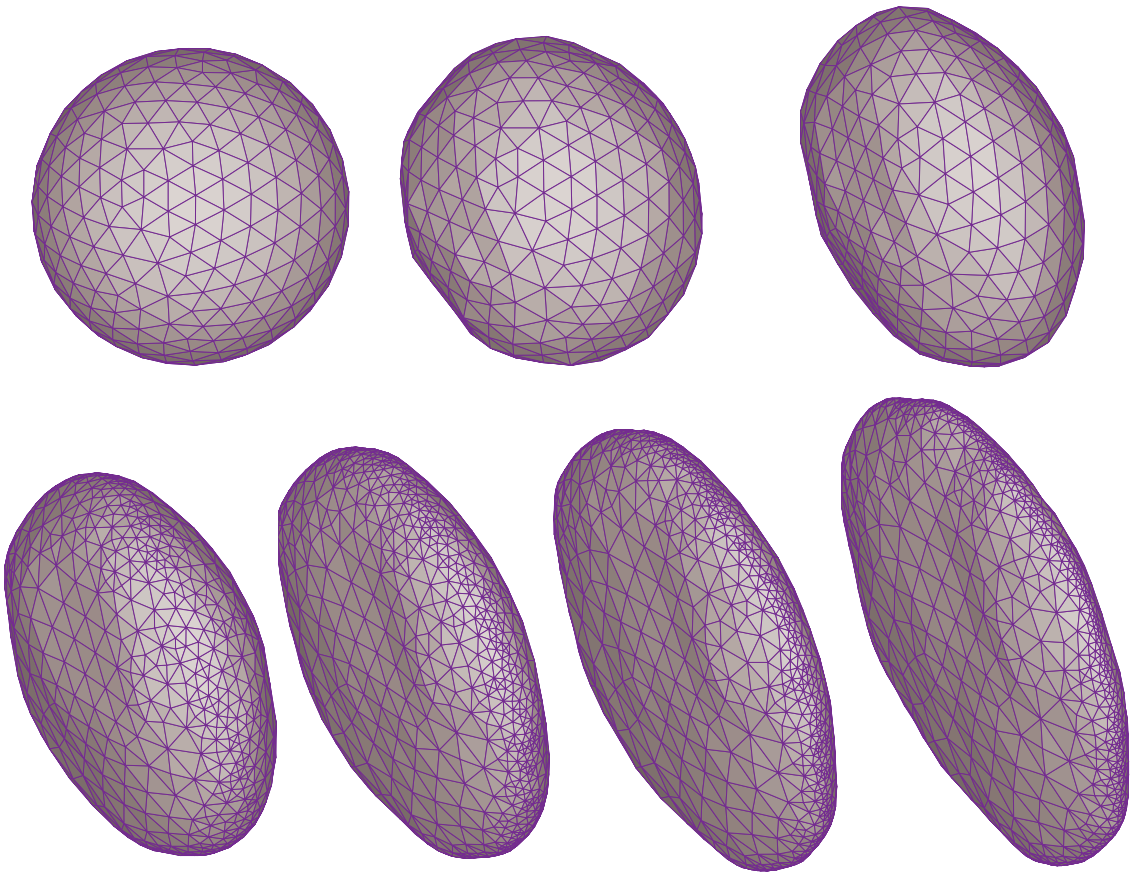

Figure 6: Droplet shapes at times: 0.0, 2.5, 5.0, 7.0, 10.0, 12.0 and 15.0